Since January 2020 Elsevier has created a COVID-19 resource centre with free information in English and Mandarin on the novel coronavirus COVID-19. The COVID-19 resource centre is hosted on Elsevier Connect, the company's public news and information website.

Chemical Engineering Science 223 (2020) 115727

Contents lists available at ScienceDirect

Chemical Engineering Science

journal homepage: www.elsevier.com/locate/ces

Baculovirus transit through insect cell membranes: A mechanistic approach

Youhong Zhang [a,b,*], Giora Enden [c], Wei Wei [d], Feng Zhou [a], Jie Chen [a], Jose C. Merchuk [e,*]

[a] School of Environmental Ecology and Biological Engineering, Wuhan Institute of Technology, LiuFang Campus, Guanggu 1st Road, Wuhan 430205 China
[b] Key Laboratory for Green Chemical Process of Ministry of Education, Wuhan Institute of Technology, LiuFang Campus, Guanggu 1st Road, Wuhan 430205 China
[c] Department of Biomedical Engineering, Ben-Gurion University of the Negev, Beer-Sheva 84105, Israel
[d] Institute of Marine Microbes and Ecospheres, Xiamen University (Xiang'an), Xiamen 361102, China
[e] Department of Chemical Engineering, Ben-Gurion University of the Negev, Beer-Sheva 84105, Israel

HIGHLIGHTS

- A novel mechanistic model of the early stages of viral infection.
- Excellent fit to experimental evidence.
- The maximum number of virions that Sf9 cells can carry: 55 viruses/cell, is reported.
- Cells that carry virions on their surface, in their interior, or both are distinguished.
- Analytical mathematical solution renders satisfactory results.

ARTICLE INFO

Article history:
Received 2 January 2020
Received in revised form 15 March 2020
Accepted 16 April 2020
Available online 25 April 2020

Keywords:
Baculovirus
Infection kinetics
Mathematical model
Infection Simulation

ABSTRACT

Baculovirus systems are used for various purposes, but the kinetics of the infection process is not fully understood yet. We investigated the dynamics of virion movement from a medium toward the interior of insect cells and established a mechanistic model that shows an excellent fit to experimental results. It also makes possible a description of the viral dynamics on the cell surface. A novel measurement method was used to distinguish between infected cells that carry virions on their surfaces, cells that carry virions in their interior, and those carrying virions both inside and on their surface. The maximum number of virions carried by a cell: 55 viruses/cell, and the time required for viral internalization, 0.8*h*, are reported. This information is particularly useful for assessing the infection efficacy and the required number of virions needed to infect a given cell population. Although our model specifically concerns the infection process of Sf9 insect cells by baculovirus, it describes general features of viral infection. Some of the model features may eventually be applicable in the studies towards palliation of the COVID-19 outbreak.

1. Introduction

The baculovirus (BV) expression vector system (BEVS) is of great interest for the production of recombinant proteins in a wide range of fields—from basic science research to the development of biomedical applications and the production of bio-insecticides (Felberbaum, 2015; Kost et al., 2005; Mehalko and Esposito, 2016; Shang et al., 2017). The production of recombinant proteins in BEVS is greatly affected by the characteristics and kinetics of the viral infection process—including, for instance, the multiplicity of infection (MOI), time of infection (TOI), cell cycle, cell line selection, and culture state (Ge et al., 2014; Kioukia et al., 1995; Lecina et al., 2006; Licari and Bailey, 1992; Monteiro et al., 2017, 2014, 2016; Nwe et al., 2006; Saito et al., 2002; Zhang et al., 2005; Enden et al., 2005), but the early events of viral infection, such as the attachment of virions to their receptors and the kinetics of their entry into the cell, are still not entirely understood. This gap hampers the development of efficient and specific genetically engineered proteins and gene therapy vectors based on BV – a goal that has lately gained much interest (Licari and Bailey, 1992; Felberbaum, 2015; Kost et al., 2005; Mehalko and Esposito, 2016; Shang et al., 2017). Since baculovirus was used for efficient gene transfer to mammalian cells in the 1990s (Boyce and Bucher, 1996; Hofmann et al., 1995), several effective baculovirus-based gene therapy vectors had been created and tested, demonstrating

* Corresponding authors at: School of Environmental Ecology and Biological Engineering, Wuhan Institute of Technology, LiuFang Campus, Guanggu 1st Road, Wuhan 430205 China (Y. Zhang).
E-mail addresses: youhong@wit.edu.cn (Y. Zhang), jcm@bgu.ac.il (J.C. Merchuk).

https://doi.org/10.1016/j.ces.2020.115727
0009-2509/

Nomenclature

Abbreviations

wt AcV1	wild type Anti-Baculovirus Envelope gp64 Monoclonal Antibody
wt AcV1-PE	wild type specific label for GP64
BV	baculovirus
BEVS	baculovirus expression vector system
MOI	multiplicity of infection
NC	nucleocapsid
TOI	time of infection
FCM	flow computed cytometry
GP64	major envelope protein of the BV
hpi	hours post infection
PFU	plaque forming unit
Sf9	(CCTCC-GDC0008) insect cell line used
SYBR	nucleic acid dye
FSC-H	forward scattering
SSC-H	side scattering
TCID50	50% tissue culture Infective Dose
PBS	phosphate-buffered saline
SYBR Green I	specific nucleic acid dye
SHIV	simian/human immunodeficiency virus
wt *AcMNPV*, CCTCC GDV114	virus used (wild type *Autographa californica* multicapsid nucleopolyhedrovirus)

Symbols

$A(t)$	virions attached to cell surface [NC/mL]
C	total cell concentration, [cell/mL]
C_i	concentration of infected cells, [cell/mL]
C_{id}	concentration of dark cells (Eq. (4)), [cell/mL]
C_{iw}	concentration of infected cells measured without permeabilization [cell/mL]
C_{ip}	concentration of infected cells measured with permeabilization [cell/mL]
C_{ipf}	final measured concentration of infected cells [cell/mL]
C_0	initial cell concentration, [cell/mL]
C_v	concentration of viable, or not infected cells, [cell/mL]
$I(t)$	number of internalized viruses at time t, [cell/mL]
k	kinetic constant for virion removal from the medium, Eq. (6), [mL/($NC \times$ h)]
$k_i^{'}$	kinetic constant for cell infection, [mL/$\left(N^2C \times h\right)$]
k_i	modified constant for cell infection, ($k_i^{'} \times$N), [mL/($NC \times h$)]
k_d	proportionality constant for dark cell appearance, defined in Eq. (19), [1/h]
k_g	kinetic constant of biomass growth [1/h]
k_w	Proportionality constant in Eq. (19), [cell/NC]
N	maximum number of virions that can attach to a cell
$r_a(t)$	rate of change of the attached virions function $A(t)$, [NC/(mL $\times$ h)]
$r_i(t)$	rate of viral internalization, [NC/(mL $\times$ h)]
$r_x(t)$	rate of virion removal from the medium [NC/(mL $\times$ h)]
t	time, [h]
t_e	time of internalization, [h]
V	concentration of virions in the medium [NC/mL]
V_f	final measured concentration of virions, [NC/mL]
V_0	initial concentration of virions, [NC/mL]
$x(t)$	concentration of viruses removed from the medium, [NC/mL]
Wc	scaling factor, [mL/cell]
Wx	scaling factor [mL/NC]
Z	cost function
β	(NC_0), Eq. (21)
δ	$k(N \cdot C_0 - V_0)$, Eq. (21)

favorable therapeutic efficacy in laboratory and preclinical phase studies (Ono et al., 2018; Mansouri and Berger, 2018; Makkonen et al., 2015; Van Oers et al., 2015). Although the entry processes and the mechanisms involving BVs infection of insect cells or transduction of mammalian cells remain poorly understood, it has been shown that a similar mechanism may mediate GP64 binding to permissive host cells (Blissard and Theilmann, 2018; Oflynn et al., 2012; Dong and Blissard, 2012) and that BVs enter insect and mammalian cells through a clathrin-mediated endocytosis (Kataoka et al., 2012; Long et al., 2006). Thus, comprehensively characterizing the kinetics underlying the early steps of BVs infection of insect cells is crucial both for improving the production of recombinant proteins in insect cells and for designing therapy vectors and enhancing gene transduction efficacy in therapeutic studies.

Mathematical modeling and simulations may serve as effective predictive tools in pursuing this goal (Licari and Bailey, 1992; Dee and Shuler, 1997; Zhang et al., 2005; Enden et al., 2005), as they allow dynamical simulation of the process and estimating variables that are hard to measure directly, such as the rate of virion internalization after its attachment to the cell. Quantitative models were also employed to simulate the infection dynamics of infectious diseases. Padmanabhan and Dixit (2011) constructed a kinetic model of hepatitis C virus (HCV) which accounted explicitly for the dependence of HCV entry target cells on CD81 expression. Iwami et al. (2012) optimized a mathematical model to describe the kinetics of the simian/human immunodeficiency virus (SHIV) infection which improved the understanding of SHIV and human immunodeficiency virus type-1 pathogenesis. Such models, and the virtual experiments that they facilitate, are useful for interpreting the mechanistic aspects of the viral infection process and may save time, manpower, and physical resources in predicting their outcomes. The main purpose of the current study was to construct such a model, focusing on the early stages of a high-MOI BV infection of insect cells (Zhang et al., 2005; Wong et al., 1996), based on and tested against experimental results.

Our model embodies an interdisciplinary integration of microbiology, biology, engineering and mathematics and sets a basic mechanistic approach to the early stages of the infection process. It disregards the effect of non-infective viral mutants which might enter the cell without infecting it. It also does not address the effectiveness of infection, which may vary depending on the elapsed storage time, mainly due to viral aggregation within the viral stocks (Jorio et al., 2006; Shen et al., 2002). As we used the same storage time in all experiments, particle aggregation did not affect the measured results. Consequently, we disregarded storage time in our model. Based on detailed and accurate measurements, our model enhances our understanding of the early BV infection process and can be potentially extended to describe the early stages of other infection processes, such as gene delivery by viruses in mammalian cells. It also provides a basis for modelling the production of foreign proteins. The present model is a first step towards the long-term goal of establishing a more elaborated model of the production process, aimed at saving time, manpower, and physical resources.

2. Materials and methods

2.1. Cells and virions

The insect cell line used in this study was Sf9 (CCTCC-GDC0008). The cells were routinely maintained in 25-cm^2 culture

T-flasks (Corning, NY) at 27 °C in SF-SFM medium (Wmbio, Shuzhou, China). For suspension cultures, the Sf9 cells were incubated at 100 rpm in triplicate in 250 mL Erlenmeyer flasks containing 60 mL of cell suspension and supplemented with 0.05% (w/v) Pluronic F-68 (Sigma, St. Louis, MO). Wild-type *Autographa californica* nucleopolyhedrovirus (wt *AcMNPV*, CCTCC GDV114) was kindly provided by Professor Qi Yipeng (Wuhan University, China).

2.2. Experimental procedure

Cells from the T-flasks were transferred to suspension cultures in Erlenmeyer flasks to decrease the lag phase in subsequent stages. When the cells in the pre-culture of the first Erlenmeyer flask reached the late exponential phase (after approximately 96*h*, depending on the initial cell density), the cultures were transferred to 12 Erlenmeyer flasks (control, i.e., mock-infected, and three different MOIs, all in triplicates) and diluted with fresh medium to a cell concentration of approximately 1.2×10^6 cells/mL. After 12*h*, these new cell cultures were considered to be in their early exponential phases, reaching a density of approximately 1.7×10^6 cells/mL. At this point, the cultures were infected with MOIs of 114, 219, or 421 BVs per cell. Note that the units of MOI used here are the ratio of viral particles to cells, as counted by a flow cytometer (Becton Dickinson, San Jose, TX), while, traditionally, it is measured as plaque-forming units (PFUs) per cell or as $TCID_{50}$/cell. The ratio of FCM counts to end-point dilution assay titers ranges from 1.0 to 9.4, with an average of 3.7 and a standard deviation of 2.4 (Jorio et al., 2006). Thus, the MOIs of 100, 200 and 400 BVs/cell used in present experiments were equivalent to 25, 50 and 100 $TCID_{50}$/cell.

2.3. Analytical methods

2.3.1. Flow cytometric detection of baculovirus titer

An improved method of FCM was used to quantify baculovirus titer, as described previously (Jorio et al., 2006; Shen et al., 2002; Brussaard, 2004). Prior to the FCM analysis, in the final 1-mL phosphate-buffered saline (PBS, pH 8.0) solution, virion samples were fixed with 0.1% (w/v) paraformaldehyde for 30 min at 4 °C and then stained with a specific nucleic acid dye, SYBR Green I, at a commercially available concentration (1×10^{-4}) for 10 min at 80 °C. Yellow-green fluorescence microspheres (1 μm in diameter, Molecular Probes, Eugene, OR) were added (as an internal reference to the BV) to the control sample (Brussaard et al., 2000). All samples were analyzed using a FACS Calibur flow cytometer (Becton Dickinson, San Jose, TX) and the threshold was set on green fluorescence (FL1-H) to eliminate the background interference.

Comparing the number of virion particles with yellow-green fluorescent microspheres, the BV titer was determined by FCM using CellQuest software (Becton Dickinson, San Jose, TX). To avoid the coincidence of viral particles (i.e., two or more particles simultaneously being within the sensing zone), the samples were diluted such that the total event rate was kept below 500 events/s.

2.3.2. Determination of infected and uninfected cells

Cells were counted with a hemocytometer using trypan blue (0.5% w/v) exclusion to distinguish dead from live cells. To experimentally monitor the early stages of the infection process and detect infection in cells to which virions attach, we directly tracked GP64—the major envelope protein of the BV, which plays a crucial role in the early stages of infection. GP64 is essential for the attachment of virions to cells in a culture and for their transport between cells in infected tissues (Monsma et al., 1996), as it is involved in the binding of the virions to host cell receptors (Hefferon et al., 1999) and acts to locally reduce the membrane pH, which triggers membrane fusion. Once the virus has entered the cell by endocytosis, GP64 is necessary for stripping the nucleocapsid from its capsid proteins and for releasing the virion into the cytosol (Kingsley et al., 1999; Markovic et al., 1998; Plonsky et al., 1999). To label GP64 specifically and thereby detect only infected cells, we used the monoclonal antibody AcV1, which binds to GP64 but does not reduce its ability to attach to cells (Kataoka et al., 2012; Hohmann and Faulkner, 1983; Volkman and Goldsmith, 1985; Dhungel et al., 2013; Granio et al., 2009). To differentiate between virions that are attached to the cell surface from those that have already entered it, we either permeabilized the cells or left them intact (see methods) assuming that AcV1 labeled BVs attaches to the cell surface in both permeabilized and non-permeabilized cells, but it penetrates only into permeabilized cells. Thus, cells can be categorized according to the following criteria: cells carrying viruses on their surface only, cells carrying viruses both on their surface and in their interior, and cells carrying virions only in their interior (where in the latter all the attachment sites have been used and all the virions have made their ingress into the cells). Two types of measurements were done on each sample, rendering different readings. Fig. 1 shows diagrammatically which cells are detected in each reading. AcV1, conjugated with a fluorescent PE.

(AcV1-PE), was used specifically against the GP64 envelope glycoprotein of the BVs, thereby labeling attached and, in the case of permeabilized cells, internalized viruses (Jacobberger et al., 1986). The infected cells were then distinguished from uninfected cells using FCM analysis. A cell was considered "infected" once the first virion attached to its surface. Thus, we identified infected cells by their high antibody fluorescence, while all other cells were considered to be uninfected (and are not distinguishable from the "dark cells" described in the text). The results of the FCM measurements of the concentrations of infected cells were analyzed by CellQuest software (Becton Dickinson, San Jose, CABD) and interpreted using the subtraction method (Sladek and Jacobberger, 1993).

The samples were taken along time from cultures infected with MOIs of 114, 219, or 421 BVs/cell (see "Infection" above), and these samples were placed into 5-mL tubes by centrifugation (5 min at 1200 rpm). Then, the supernatants were aspirated, and the remaining cells were fully re-suspended by adding 3 mL of PBS (pH: 7.2) with vortex. After washing the cell samples twice, the cell samples were fixed by adding 100 μL of a paraformaldehyde solution (1% v/v final concentration) and vortexing, then stored at 4 °C in the dark for 30 min. To count the number of permeabilized infected cells, the samples were washed once with 3 mL PBS (pH: 7.2) and then added with 100 μL of a permeabilization reagent (reagent B, Fix & Perm kit, Invitrogen, Grand Island, NY) and 5 μL of AcV1-PE (eBioscience, Santiago, CA). To count the number of non-permeabilized infected cells, the samples were stained with 5 μL AcV1-PE without adding the permeabilization reagents. After a 30 min incubation at 4 °C in the dark, the cell samples were washed again. Finally, to obtain the optimal fluorescence signal, the cell samples were examined by FCM within 30 min. The infected and uninfected cells were detected using the scatter plot with forward scattering (FSC-H) versus side scattering (SSC-H), and then the ratio of infected to total cells was analyzed by the BD CellQuest software. Control cell samples were treated using the same steps, but without adding AcV1-PE (data not shown).

3. Results, modeling and discussion

3.1. Attachment of virions to cells

We began by establishing the capacity of Sf9 cells to carry *Autographa californica* multicapsid nucleopolyhedrovirus (AcMNPV) – an important reference for MOI optimization. We detected the vir-

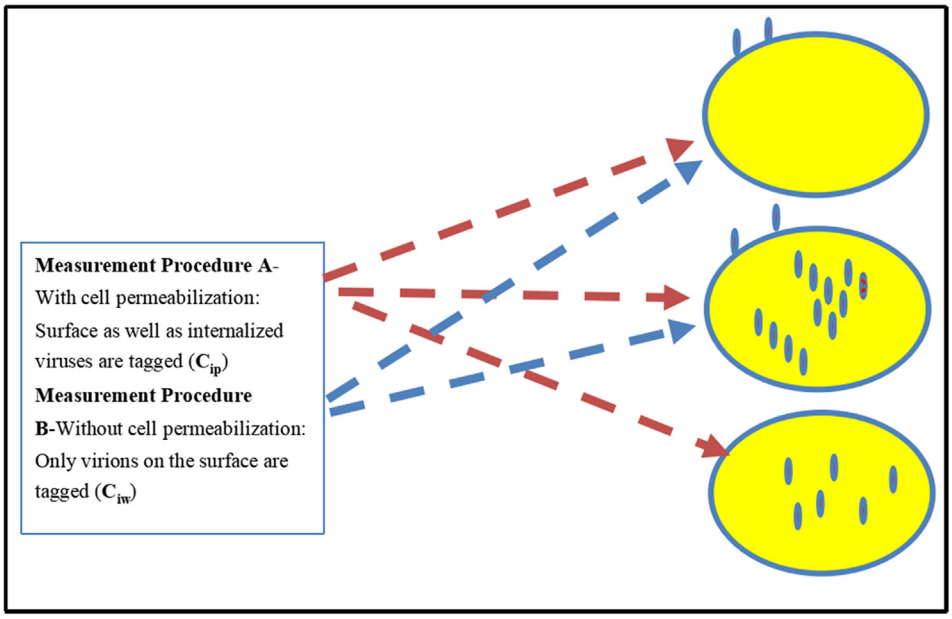

Fig. 1. Three cells in the different states considered are shown: A cell carrying viruses on its surface only, a cell carrying viruses both on its surface and in its interior, and a cell carrying virions only in its interior. Two types of measurements were done on the same sample producing different readings: (A) With cell permeabilization (Surface as well as internalized viruses are detected) and (B) Without cell permeabilization (Only virions on the surface are tagged).

ion titer by flow cytometry (FCM), using the fluorescent dye SYBR Green I to stain the nucleic acids of the virions (Jorio et al., 2006; Shen et al., 2002; Brussaard, 2004; Brussaard et al., 2000). The Sf9 cells were infected with AcMNPV at MOIs of 114, 219, or 421 BVs/cell, and the obtained virion and cell profiles are shown in Fig. 2. It should be kept in mind that generally baculovirus infections are reported in units of $TCID_{50}$/cell. In such case the usual range of MOI in a Baculovirus infection is 10–50. In the present case we are using FCM measurements. The ratio of FCM counts to end-point dilution assay titers ranges from 1.0 to 9.4, with an average of 3.7 and a standard deviation of 2.4 (Jorio et al., 2006). Thus, the MOIs of 100, 200 and 400 BVs/cell used in present experiments were almost equivalent to 25, 50 and 100 $TCID_{50}$/cell.

The maximum number of virions that can attach to a cell, N, is defined here as:

$$N = \lfloor V(0) - V_f \rfloor / C_{ipf} \tag{1}$$

where it is assumed that MOI $\geq N$.

Here V_f is the final measured concentration of virions in the medium, C_{ipf} is the final measured concentration of infected cells 9 h post-infection (*hpi*), as shown in Fig. 2 and Table 1. The sub-index p indicates cell samples which were treated with permeabilizing reagents., C_{ipf} is also an upper bound of the concentration of the infected cells at any time point. For MOIs = 114, 219, and 421, we found N = 52.8, 55.3, and 58 attachment sites per cell, respectively. In principle it is accepted here that N is a property of the cell, which means that a cell has finite attachment sites that should be identical for all cells and under all conditions. In our experimental results we found a small difference between the three MOIs, with a standard deviation lower than 5% for a mean N of 55, which may be considered as experimentally acceptable. Thus, we suggest using N = 55 for *Autographa californica* at any MOI. When this model is applied to anti-tumor therapy with baculovirus vectors, N would be the basis for calculating the upper limit of viral concentration required to deliver a foreign gene to target cells. The optimal dosage per cell should be between zero and N. The desired dose per cell (MOI) can be defined as that which maximizes the expectancy of treated cells with minimal costs.

3.2. Kinetic modelling

3.2.1. Growth kinetics of non-infected cells

In the initial stage of the study, we characterized the kinetics of non-infected Sf9 cells, which were grown under the same conditions as those used in the infection experiments (see Methods in the Attachments), but without BV infection. It was found that the simple first-order growth rate fits satisfactorily the collected data. The use of more sophisticated kinetic forms is therefore unnecessary. The kinetic expression for the growth of non-infected cells is:

$$dC/dt = k_g C \tag{2}$$

$$C(0) = C_0$$

The solution of this equation is:

$$C(t) = C_0 exp(k_g \cdot t) \tag{3}$$

where C is the cell concentration, t is time, and k_g is the growth rate factor. Regression of expression (3), based on all experimental data points in a 60h experiment, yielded $k_g = 0.022\ \left[h^{-1}\right]$. This kinetic rate constant was used in the mathematical model described below. The value is lower than data reported previously for these cells, but it should be kept in mind that anyway the growth rate of the cells is sensibly lower that the infection rate. This consideration is reinforced further by the success of the assumption of constant cell concentration rate presented in Section 3.5.

3.2.2. Dynamics of the early stages of infection

The dynamics of the early stages of the infection process in Sf9 cells are shown in Fig. 3 for MOIs = 114, 219, and 421. The percentage of infected cells, as evaluated without permeabilization, C_{iw}, increased until 4 *hpi*, reached a maximum of 79%, and then slowly decreased to 65% at 9 *hpi*. This maximum will be explained below in terms of the balance between virus attachment and virus internalization. In contrast, the percentage of the infected cells, as evaluated when permeabilizing reagents were used in the analysis, C_{ip}, increased monotonically, reached a maximum of 97%, and then, either remained unchanged, or moderately increased to a plateau.

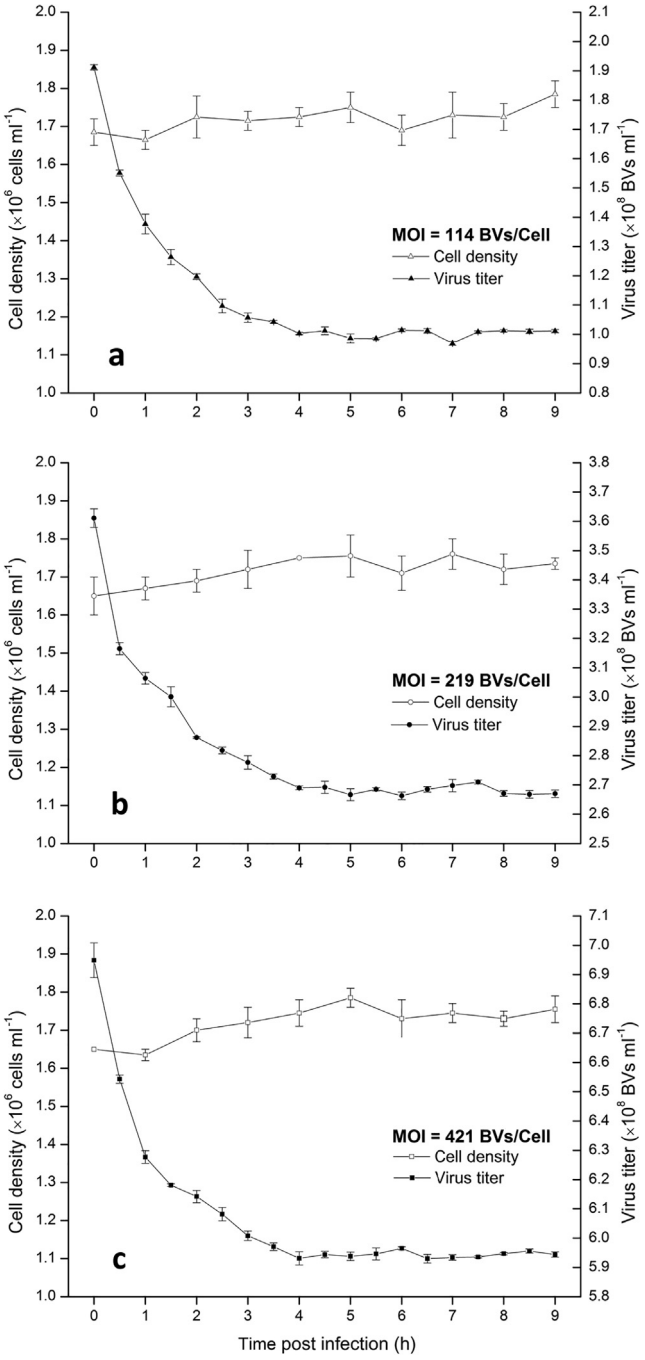

Fig. 2. Main experimental data. Changes in the cell density (empty data points, left ordinate) and virion titer (filled data points, right ordinate), from 0 to 9 *hpi*, at MOIs of 114 (a), 219 (b), and 421 (c) BVs/cell. Cell growth is observed only during the first 4 h post infection. Each data point represents the mean ± SD of three independent experiments.

This effect was observed with only minor differences between the three examined MOIs (although higher MOIs resulted in a slightly higher C_{ip}), suggesting that almost all cells were infected by or before approximately 6 *hpi*. C_{ip} denotes the number of infected cells carrying virions on their surface and/or their interior. C_{ip} is an essential indicator in pathopoiesis of viruses. The higher C_{ip}, the severe the incidence of diseases. In the early stage of virus infection, the rate of change of C_{ip} is similar to the transduction dynamics of target cells with viral vectors in an *ex vivo* therapy. In the same way the transduction efficiency of viral vectors plays a fundamental role in improving the therapeutic efficacy of a gene therapy program (Asad et al., 2017; Kalesnykas et al., 2017; Sinn et al., 2017; Espirituramirez et al., 2018); C_{ip} could be considered a key parameter in gene therapy treatment based on viral vectors.

The difference between the values of C_{ip} and C_{iw} corresponds to the apparition of a new type of cells: those that have already internalized the maximum possible number of virions, N. In an FCM analysis, these cells show a very weak fluorescence, similar to that of uninfected cells, because they do not internally carry an AcV1 conjugated with a fluorescent phycoerythrin (PE). Therefore, it is difficult to distinguish between them and uninfected cells, unless they are treated with permeabilizing agent – which would make them strongly fluorescent. If we denote their concentration as C_{id}, then

$$C_{id} = C_{ip} - C_{iw} \tag{4}$$

The profiles shown in Fig. 3 indicate that C_{id} remains very low during the first hour post infection, but then begins to increase; this slow initial response (as manifested by the coincidence of C_{ip} and C_{iw}) is presumably because either none or very few of the infected cells have internalized virions to their full capacity (N) at this stage. C_{id} is expected to continue to increase and eventually reach values close to C_{ip} as C_{iw} reaches very low values due to full internalization of all the virions that had attached to the cell surface. C_{id} indicates the amount of cells with fully internalized virions, and the change in C_{id} reflects the infection stage. The higher C_{id}, the more advanced is the infection stage.

3.2.3. Modeling the dynamics of the early stages of infection

To model the dynamics of the early infection process, we used the following variables: x [virions/mL], the concentration of virions removed from the medium; C_v [cells/mL], the concentration of uninfected cells; and C_i [cells/mL], the concentration of infected cells. We considered the total concentration of cells in the system to be equal to the sum of concentrations of the uninfected and infected cells:

$$C = C_v + C_i \tag{5}$$

The infection process is viewed here as two serial steps: the first is the virion–cell encounter and its attachment to the cell surface, as defined in Eqs. (6) and (9); the second step consists of the internalization of the virion into the cell, assumed here to last a certain time, t_e, as reflected in Eqs. (9)–(21). In addition, we assume that (1) all attachment sites are identical and the behavior of all virions is essentially identical; (2) the internalization time t_e is identical for all cell-virion couplings; (3) after infection, virions continue to attach to cells as long as the saturation point (N) is not reached; (4) each attachment site can be used only once; (5) the time between consecutive virion attachments to the same cell is shorter than t_e. The latter bears the simplifying assumption that after the first virion attachment to each untreated cell, it will appear as "infected" until all its N attachment sites are used and all its surface virions internalized.

3.2.4. Kinetics of virion attachment

One of the simplest ways to depict macroscopically the mechanism of virion attachment to cells is to assume that the rate of attachment is proportional to both the number of free virions and the number of unused attachment sites on the cell.

Denote the initial virion concentration in the medium as V_0 and the number of virions removed from a unit volume of the medium (via attachment to cells) as $x(t)$. The concentration of free virions in the medium is therefore, $V = V_0 - x$. Assuming that the rate of virus attachments is proportional both to free virus concentration

Table 1
Experimental data on free viruses in the medium and the infected cell concentrations for each MOI.

	MOI: 114 ($C_0 = 1.69 \times 10^6$ cells mL^{-1})		**MOI: 219** ($C_0 = 1.65 \times 10^6$ cells mL^{-1})		**MOI: 421** ($C_0 = 1.65 \times 10^6$ cells mL^{-1})	
hpi h	Infected cell titer ($\times 10^6$ cells mL^{-1})	Virus titer ($\times 10^8$ BVs/mL)	Infected cell titer ($\times 10^6$ cells mL^{-1})	Virus titer ($\times 10^8$ BVs/mL)	Infected cell titer ($\times 10^6$ cells mL^{-1})	Virus titer ($\times 10^8$ BVs/mL)
0	0.000	1.912	0.000	3.611	0.000	6.949
1	0.992	1.377	1.060	3.064	1.080	6.277
2	1.255	1.197	1.323	2.862	1.330	6.142
3	1.463	1.057	1.504	2.777	1.563	6.008
4	1.544	1.003	1.607	2.69	1.645	5.931
5	1.586	0.986	1.653	2.667	1.719	5.938
6	1.559	1.014	1.634	2.663	1.694	5.965
7	1.613	0.969	1.696	2.698	1.707	5.934
8	1.620	1.012	1.674	2.671	1.705	5.947
9	1.704	1.011	1.700	2.67	1.734	5.944

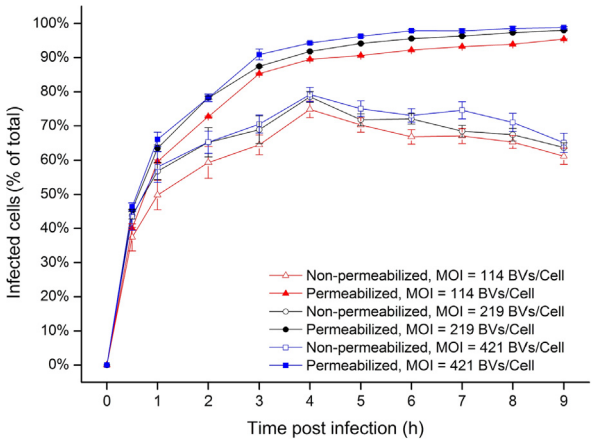

Fig. 3. The infection process. Evolution of the concentrations of infected cells as detected in non-permeabilized cells (empty data points) and permeabilized cells (filled data points), from 0 to 9 *hpi*, at MOIs of 114 (red), 219 (black) and 421 (blue) BVs/cell. The number of infected cells increases monotonically to approximately 100% when measured on permeabilized cells but only reaches approximately 70% when measured on cells without permeabilization. Each data point represents the mean ± SD of three independent experiments. (For interpretation of the references to colour in this figure legend, the reader is referred to the web version of this article.)

and to the concentration of attachment sites, the differential equation describing the adsorption rate of virions can be written as:

$$dx/dt = k \cdot [V_0 - x(t)] \cdot [N \cdot C(t) - x(t)] = r_x \quad 0 < t \tag{6}$$

where $C(t) = C_v(t) + C_i(t)$ is the total cell concentration t hours after TOI, and

$$\text{at } t = 0 (= TOI), \quad x(0) = 0. \tag{7}$$

Eq. (6) therefore states that the rate of virus attachment is proportional both to the number of free virus and to the number of free attachments sites. In the equation, k [mL/(attachment sites × h)] is the attachment kinetic constant, and the number of free attachment sites per unit volume in the cell culture t hours after TOI equals $[N \cdot C(t) - x(t)]$.

3.2.5. Cell infection as detected in permeabilized cells

The material balance on the infected cells in the system yields:

$$dC_{ip}/dt = k_i' \cdot (V_0 - x) \cdot N \cdot C_v \quad 0 < t \tag{8}$$

which assumes that rate of increase of infected cells concentration is proportional to both the free virus and viable cells concentrations.

In Eq. (8), C_{ip} denotes the concentration of infected cells, treated with permeabilizing reagents, while k_i' is the kinetic constant of infection. Defining $k_i = k_i' \cdot N$, we obtain

$$dC_{ip}/dt = k_i \cdot (V_0 - x) \cdot C_v \quad 0 < t \tag{9}$$

where $k_i = k_i$ [mL/(number of virions × h)].

$$\text{At TOI}, \quad C_{ip}(0) = 0 \tag{10}$$

A balance on the pool of viable cells will include a cell growth term, already shown in Eq. (1) to be a first-order process with a kinetic constant k_g, and a second term for viable cell depletion by infection:

$$dC_v/dt = k_g \cdot C_v - k_i \cdot (V_0 - x) \cdot C_v \tag{11}$$

$$\text{At TOI}, \quad C_v(0) = C(0) = C_0 \tag{12}$$

where C_0 for each MOI is shown in Table 1.

Eq. (11) indicates that the accumulation of viable cells is balanced by the difference between the generation of new cells and the depletion of the pool of viable cells due to infection. Eqs. (5)–(12) were solved to obtain concentration profiles of the virions removed from the medium, x, infected cells, C_i, and viable cells, C_v. The results of the complete model are detailed below.

3.2.6. Cell infection as detected in non-permeabilized cells

In this case, cells containing only internalized virions cannot be distinguished from uninfected cells, since AcV1 conjugated with a fluorescent PE cannot enter into non-permeabilized cells. Assuming that the internalization time, t_e, is identical for all virions, we can calculate $A(t)$, i.e., the number of virions (per unit volume of the medium) attached to cell surfaces (and, therefore, detectable) at any given time. This value is equal to $x(t)$ for $t < t_e$, and is equal to the difference between the number of virions that were attached to the cells between $(t - t_e)$ and t for $t_e \le t$, since virions that arrived earlier than $(t - t_e)$ have already been internalized and cannot be detected. Therefore,

$$A(t) = \begin{cases} x(t) & 0 \le t < t_e \\ x(t) - x(t - t_e) & t_e \le t \end{cases} \tag{13}$$

Denoting by $I(t)$ the number of internalized viruses at time t per unit volume of the medium, we obtain:

$$I(t) = \begin{cases} 0 & 0 \le t < t_e \\ x(t - t_e) & t_e \le t \end{cases} \tag{14}$$

The rate of change of $A(t)$, $r_a(t)$, at time t, is:

$$r_a(t) = d/dt \begin{cases} x(t) & 0 \le t < t_e \\ x(t) - x(t - t_e) & t_e \le t \end{cases} \tag{15}$$

And, following, Eq. (6):

$$r_a(t) = \begin{cases} r_x(t) & 0 \le t < t_e \\ r_x(t) - r_x(t - t_e) & t_e \le t \end{cases} \tag{16}$$

The rate of viral internalization, $r_i(t)$, at a time t, is:

$$r_i(t) = dI(t)/dt = d/dt \begin{cases} 0 & 0 \le t < t_e \\ x(t - t_e) & t_e \le t \end{cases}$$
$$= \begin{cases} 0 & 0 \le t < t_e \\ k \cdot [V_0 - x(t - t_e)] \cdot [N \cdot C(t - t_e) - x(t - t_e)] & t_e \le t \end{cases} \tag{17}$$

The next step is to associate the virion attachment and internalization processes to the measured infected cell concentrations, C_{ip} and C_{iw}. This association, expressed in Eq. (4), can be obtained by using the difference between the two above mentioned variables, C_{id}, which represents the concentration of the infected non-permeabilized cells that have already internalized all the attached virions. The relationship between virion internalization and C_{id} is by no means simple. The internalization rate, r_i, is the result of a very large number of attachment events of viruses to cells. At a given time, the states of these cells vary considerably, ranging from non-infected (a very small fraction) to infected cells that already have attached various numbers of virions, up to N. The darkening of any detected cell occurs only after the cell has accumulated N attachment events and a time t_e has passed since the last such event. Considering the multiple possibilities in the process of occupying a cell to its maximum capacity N, two extreme patterns can be imagined: in one extreme, the distribution of virions among the cells is completely homogeneous: at any point in time, the number of virions in each cell is identical and, consequently, no cell darkening is observed until the very final stages of the process. In such a case, the profile of $C_{id}(t)$ would be zero until the very end of the process. On the other extreme, the virions are distributed among the cells in an orderly fashion, such that attachment to a new cell does not occur before the previously infected cell is fully saturated, i.e., at any time $t \geqslant t_e, C_{id}(t) = \left\lfloor \frac{x(t-t_e)}{N} \right\rfloor$.

Where $\lfloor x \rfloor$ denotes the "whole value function" (also called the "floor function"), which returns the largest integer that is smaller than or equals to x (rounded down). It follows that, for any $t \geq t_e$,

$$C_{id}(t) = C_{ip}(t) - C_{iw}(t) \le \left\lfloor \frac{x(t - t_e)}{N} \right\rfloor \le \frac{x(t - t_e)}{N} \tag{18}$$

A crude approximation to $C_{id}(t)$ is made here by assuming that the concentration of darkened cells is proportional to $x(t - t_e)$ for $t \geq t_e$. Noting that, for $t < t_e, C_{iw}(t) = C_{ip}(t)$, we obtain:

$$C_{id}(t) = C_{ip}(t) - C_{iw}(t) = \begin{cases} 0 & 0 \le t < t_e \\ k_w x(t - t_e) & t_e \le t \end{cases} \tag{19}$$

3.3. Calculations

The solution of this model, represented in equations (6–19), was fitted to the experimental data and the kinetic parameters k and k_i, k_w, and t_e were determined. The optimization was accomplished using the MATLAB and Polymath codes. The optimized parameters are shown in Table 2.

As the table indicates, both k and k_i change with MOI. The similarity of the values of k and k_i at each MOI indicates that the sensitivity of the system to the instantaneous number of available attachment sites is weak, as we further discuss below (in the "constant C" model). In contrast, both k_w and t_e show a very small dependence on MOI. This indicates that once initiated, the infection process is not influenced by the viral concentration in the medium.

Eqs. (6)–(13) were solved numerically using MATLAB and the parameters were evaluated with respect to the measured data in the time interval $0 \le t \le 3h$. Fig. 4 shows the measured and calculated values of x, i.e., the number of virions bound to the cells along time, and Fig. 5 shows the predicted and measured profiles of C_{ip}, C_{iw}, and C_v for each of the three MOIs. An excellent fit was found between the model and the experimental data in all cases, supporting our basic assumptions and the mechanistic approach. In Figs. 6a and 6b, we used the calculated parameters to extrapolate the numerical solution for MOI = 219 to $t = 9h$. The solution compares well with the experimental results even at this extended range. Similar results were obtained for MOIs = 114 and 421 (data not shown).

3.3.1. Parameter evaluation and sensitivity analysis

Eq. (6)–(19) were solved numerically and the obtained solution was used to evaluate the model parameters $k, k_i, k_w,$ andt_e by minimizing the sum of the squares of the differences between the model predictions and the respective experimental measurements of C_{ip}, C_{iw}, and x in the interval $0 < t \le 3h$. Since the virion and cell concentrations differ by three orders of magnitude, the convergence criterion was applied with respect to the scaled variables. The variable x was scaled with respect to $(N \times C_0)$, which is approximately the maximal possible number of attachment sites on all the cells (see Eq. (22) below). Each of the cell concentrations C_{ip} and C_{iw} was scaled with respect to C_0.

Scarcity of experimental data hindered the implementation of statistical analysis to determine confidence intervals of the evaluated parameters. Instead, the sensitivity of the model to parameter perturbations was analysed by evaluating the relative change in the cost function in response to parameter perturbations. The values of $k, k_i, k_w,$ andt_e were perturbed sequentially downwards and upwards from their base-case values. The relative effects of these perturbations on a cost function,

$$Z = \sqrt{\sum_i Wc\left(C_{ip} - \overline{C_{ip}}\right)^2 + \sum_i Wc\left(C_{iw} - \overline{C_{iw}}\right)^2 + \sum_i Wx(x_i - \overline{x_i})^2}$$

are demonstrated in Table 3 for MOI = 114.

Z was minimized with respect to the parameters k, k_i, k_w, and t_e. Here the barred variables are the experimentally measured variables, i is the time index; $Wc = {C_0}^{-1}$ and $Wx = 1/(C_0 \times N)$ are the scaling factors. Clearly, the model is sensitive to changes in k_w. On the other hand, the general agreement between the fitted values and the respective experimental values, suggests that the assumptions on which the mechanistic model is based on are satisfactory. In particular the homogeneity of t_e also supports this assertion. However, both t_e and k_w are practically independent of the concentration of virions in the medium. The results for t_e,

Table 2
Optimal values of the model parameters for each MOI.

MOI [NC/cell]	t_e [h]	k_w [cell/NC]	k_i [cc/(NC × h)]	K [cc/(NC × h)]
114	0.8	0.0055	5.1×10^{-9}	5.3×10^{-9}
219	0.79	0.0048	2.9×10^{-9}	2.7×10^{-9}
421	0.67	0.0045	1.6×10^{-9}	1.6×10^{-9}

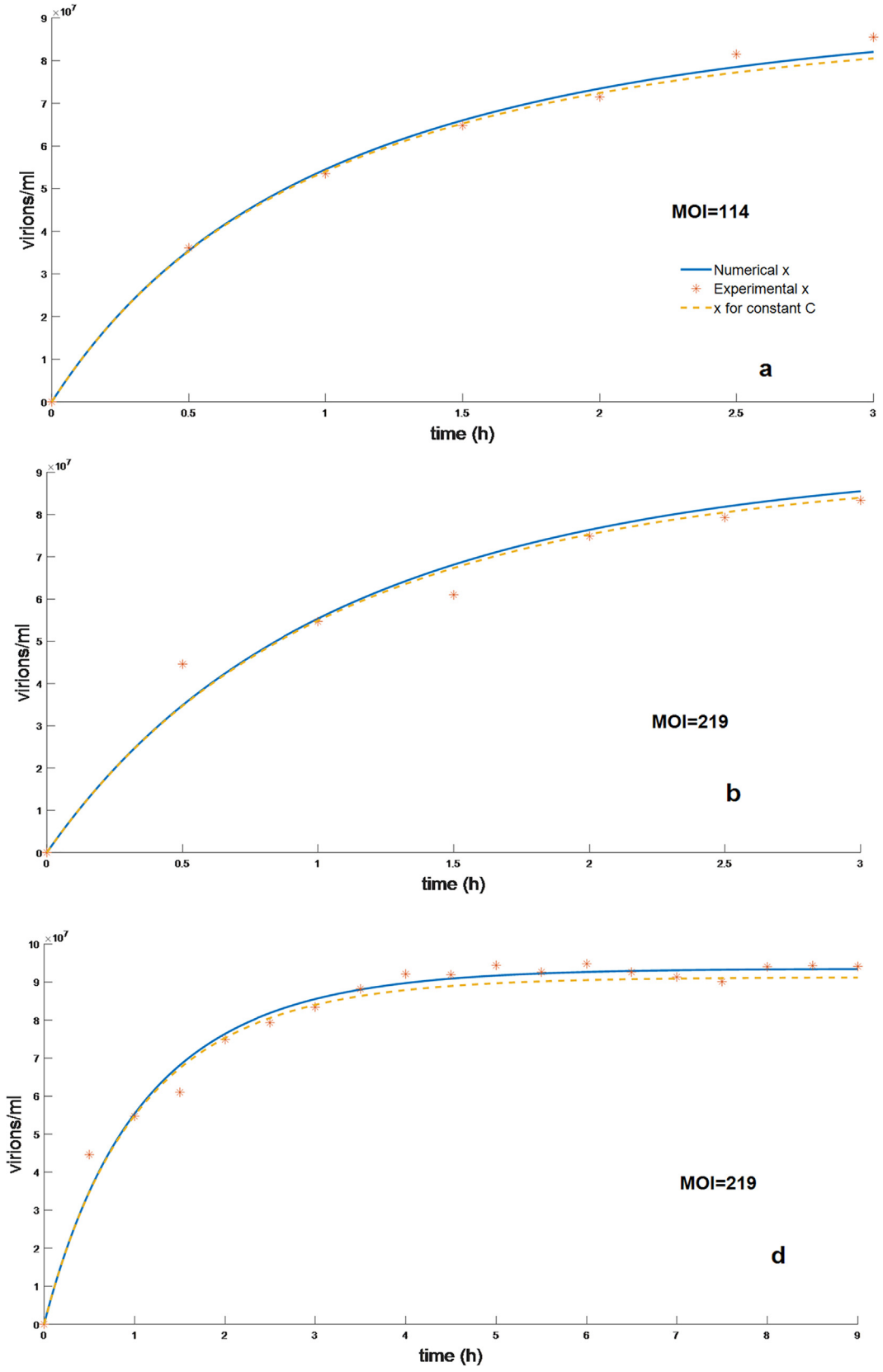

Fig. 4. Modeling results. Comparison between the experimentally measured data points of x, the virions bound to the cells (either on their surface or internalized), and the corresponding predicted values (continuous lines) at MOIs of 114 (a), 219 (b), and 421 (c). The model offers a satisfactory fit to the experimental findings. Each data point represents the mean ± SD of three independent experiments. Panel (d) demonstrates an extrapolation of the numerical solution (for MOI = 219) to $t = 9h$. Solid lines represent the complete model (Eqs. (7)–(20)) and dashed lines represent the model predictions, assuming a constant cell concentration.

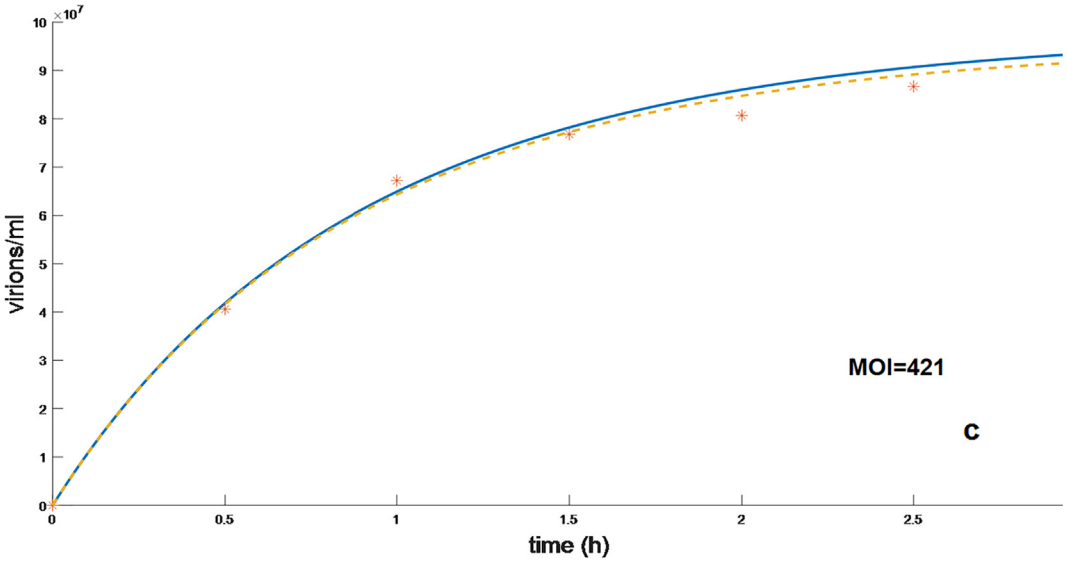

Fig. 4 (*continued*)

which are within the range of time usually observed in cell infection processes, confirm our assumption that t_e can be related to as a constant. The fact that all examined MOIs render the same t_e indicates that the internalization process is a property dependent on biological processes occurring on the cell surface and in its interior regardless of the virus concentration in the medium. Hefferon et al. (1999) found that *Orgyia pseudotsugata* multicapsid nucleopolyhedrovirus (OpMNPV) virions entered *Spodoptera frugiperda* Sf9 cells with a half-time of approximately 12.5 min. Their results differed from the results in the current study with the AcMNPV-Sf9 system shown in Table 2. This indicates that different Baculovirus may have different internalization half-time value. Since the internalization time for each specific virus-host system is expected to be a characteristic constant, it seems that viral vectors with shorter internalization times would have some advantages in gene therapy, since they enter host cells more rapidly while the cells are robust. Therefore, the estimation of the internalization time for any potential virus-host combinations may be very important. The very low value of the constant k_w indicates that the actual accumulation rate of dark cells dC_{id}/dt is substantially lower than the floor function shown in Eq. (18), and yet follows a similar pattern, given the quality of the fit.

3.4. Simulation of the dynamics on the cell surface

Based on the results shown above, a crude approximation to dC_{id}/dt can be made assuming that the generation rate of darkened cells is proportional to r_i:

$$dC_{id}/dt = k_w \cdot r_i(t) = k_w \begin{cases} 0 & 0 \le t < t_e \\ k \cdot [V_0 - x(t-t_e)] \cdot [N \cdot C(t-t_e) - x(t-t_e)] & t_e \le t \end{cases} \quad (20)$$

As an example, Fig. 6**a** demonstrates the typical dynamics of the system variables $x(t)$, $A(t)$, and $I(t)$ in the case of MOI = 114 (see below), using the obtained values of the parameters t_e and k_w (shown in Table 3).

During $0 \le t < t_e$, $A(t)$ coincides (and increases) with $x(t)$. At $t = t_e$ (the onset of internalization), $I(t)$ begins to increase and the number of viruses on the surface, $A(t)$, begins to decrease sharply. Eventually, $A(t)$ will approach zero as $I(t)$ converges to x. Despite the abrupt transition at t_e, due to the discontinuity of our model at that time, the general form of the profiles portrays a clear picture of the dynamics of the virions at the surface of the cells.

Fig. 6(b) shows the rates of virion attachment r_x, virion internalization r_i, and the rate of change in the number of virions attached to the cell surface, r_a.

A noticeable discontinuity of r_a is observed at $t_e = 0.8$, due to the first occurrence of internalization. The shift in the internalization rate at $t = t_e$ is in agreement with our experimental observations, which were based on the measured profiles of C_{ip} and C_{iw}. The model also indicates that, near 4 *hpi*, the difference between r_i and r_a becomes very small, as saturation is approached and the process nears convergence.

Despite the simplifications made, the model provides a reasonable prediction and can be considered a first approximation to the rate of viral internalization, on which experimental data are scant. Some of the features in the present model may eventually be applicable in the studies towards palliation of the COVID-19 outbreak (Zhu et al., 2020; Binnicker, 2020)

3.5. Approximation based on constant cell concentrations

The low growth factor, $k_g = 0.022$, suggests that the cell concentration, C may be treated as nearly constant at the range $0 \le t \le 3h$. This observation is further supported by the experimental behavior of the cell concentration shown in Fig. 6. In this section, we neglect the changes in C and consider it to be a constant equal to C_0. In this case, k_g is set to zero and Eqs. (6)–(12) can be integrated analytically to yield a closed-form solution for x, C_{ip}, C_{id}, C_{iw}, and C_v.

$$x(t) = \beta V_0 [exp(\delta t) - 1] / [\beta \cdot exp(\delta t) - V_0] \quad (21)$$

where $\beta = NC_0$; $\delta = k_c(NC_0 - V_0)$, and k_c is equivalent to k in Eq. (5).

The closed-form solutions of C_{ip}, C_v, C_{id} and C_{iw} are shown in the Appendix A.

Next, we used the closed-form solution with the parameters shown in Table 3. The simplifying assumption introduces very little change in the solution and can apparently be used safely. Moreover, the closeness of the dashed line (representing the constant-C model) to the solid line in Fig. 6 proves that the error in using the constant-C model introduces very small errors (possibly within experimental uncertainty).

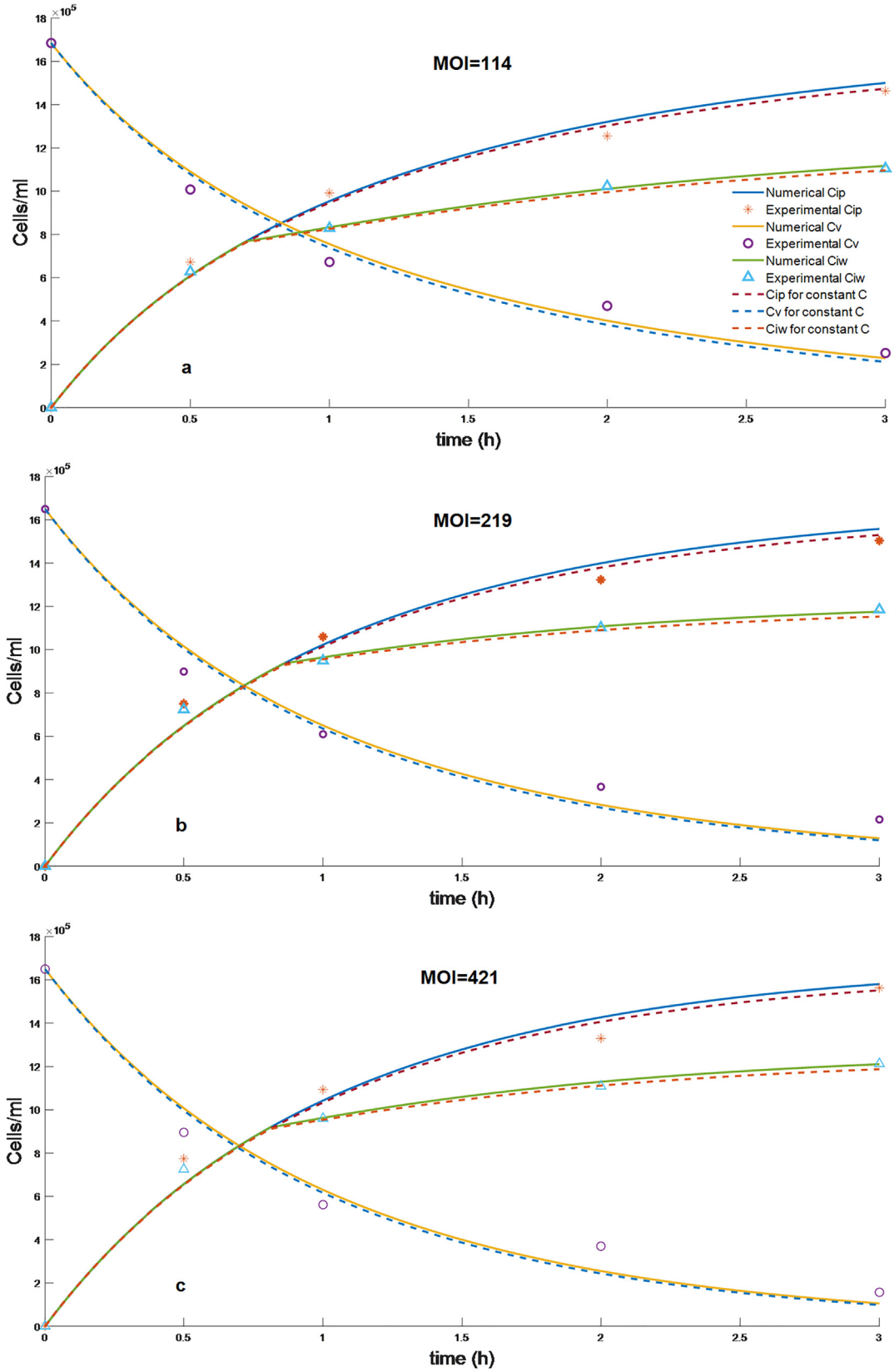

Fig. 5. Modeling results. Comparison of the experimentally measured (points) and calculated (continuous lines) values of C_{ip} (permeabilized infected cells), C_v (viable cells) and C_{iw} (non-permeabilized infected cells) at MOIs of 114 (a), 219 (b), and 421 (c). The model fits satisfactorily to the experimental findings. Each data point represents the mean ± SD of three independent experiments. Panel d demonstrates an extrapolation of the numerical solution (for MOI = 219) to $t = 9h$. Solid lines represent the complete model (Eqs. (7)–(20)) and dashed lines represent the model predictions assuming a constant cell concentration.

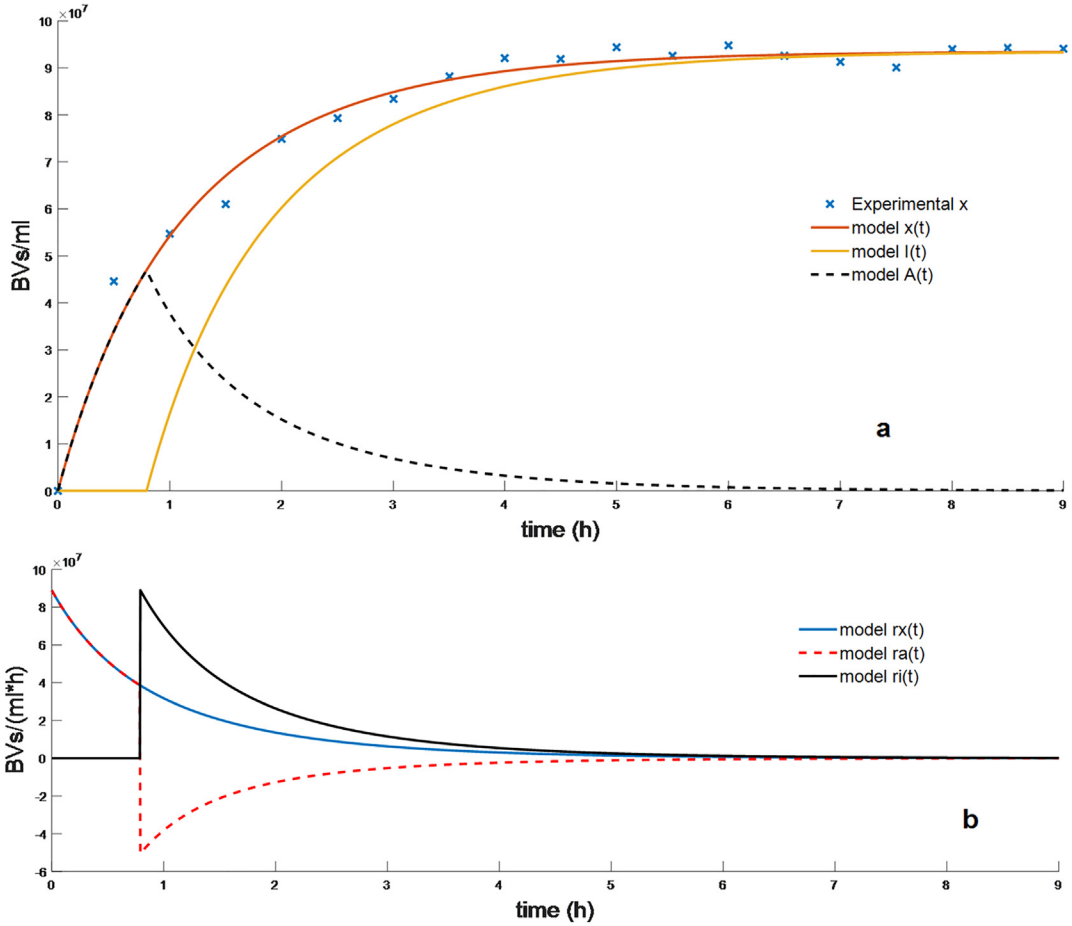

Fig. 6. Virus dynamics. (a) Temporal profiles of virions bound to the cells, $x(t)$; virions on the surface of the cells, $A(t)$, and internalized viruses, $I(t)$. (b) Comparison of the rate of virion removal from the medium, r_x; the rate of virus internalization, r_i; and the rate of change of virions found on the surface of the cells, r_a, based on the approximation in Eq. (20).

Table 3
Sensitivity analysis.

k $[mL/(NC \times h)]$	k_i $[mL/(NC \times h)]$	k_w $[cell/NC]$	t_e $[h]$	Relative change in cost function (%)
5.3×10^{-9}	5.1×10^{-9}	0.0055	0.8	0 (base values)
$5.3 \times 10^{-9} + 0.3 \times 10^{-9}$	5.1×10^{-9}	0.0055	0.8	2.2
$5.3 \times 10^{-9} - 0.3 \times 10^{-9}$	5.1×10^{-9}	0.0055	0.8	2.15
5.3×10^{-9}	$5.1 \times 10^{-9} + 0.3 \times 10^{-9}$	0.0055	0.8	2.2669
5.3×10^{-9}	$5.1 \times 10^{-9} - 0.3 \times 10^{-9}$	0.0055	0.8	1.6424
5.3×10^{-9}	5.1×10^{-9}	0.0055 + 0.0005	0.8	9.4741
5.3×10^{-9}	5.1×10^{-9}	0.0055 − 0.0005	0.8	14.0371
5.3×10^{-9}	5.1×10^{-9}	0.0055	0.8 + 0.1	1.3534
5.3×10^{-9}	5.1×10^{-9}	0.0055	0.8 − 0.1	1.7015

Note that the asymptotic value of $x(t)$,

$$\lim_{t\to\infty} x(t) = \beta = NC_0, \tag{22}$$

is independent of the kinetic constant k_c. In fact, this is the total number of attachment sites on the cells, as might be expected. As defined above, $x(t)$ is the number of virions per unit volume that have been captured by cells between 0 and t. It reaches maximum when all cells are saturated by N virions. N is a constant, specific to each virus-host system

The approximated solution, based on a constant value of the total cell concentration, appears to be successful for our set of initial conditions. The solution of Eq. (6) can be replaced by the closed-form expression given above (Eq. (21)) without noticeable changes in the predictability capacity of the model.

4. Conclusions

In the present multi-disciplinary research, we propose a mathematical model of the early-stage kinetics of Sf9 cell infection by BV, based on and tested against experimental results. To the best of our knowledge, this is the first time that the monoclonal antibody AcV1 is used to label GP64 in order to distinguish between infected and uninfected cells at different stages of virion attachment/internalization using FCM. We used MOIs of 114, 219, and 421. The maximum number of virions that can attach to a cell, N, which is crucial for planning a high MOI process, was evaluated for *Autographa californica* and found to be 55. In general, N is a significant reference for investigating the required dosage of the viruses in gene therapy schemes. The virus-host dependent constant t_e is an important characteristic of the internalization pro-

cess. Some variables, such as C_{ip}, C_{id} and $x(t)$, in our model have great significance in describing the kinetics of processes like protein production and gene therapy by baculovirus vectors.

The mathematical solution of our model shows a satisfactory fit to the experimental measurements of virion removal from the medium and the concentration profiles of the infected cells and explains the first stage dynamics in cell infection. An FCM-mediated comparison of the infection dynamics with and without cell permeabilization enabled us to distinguish between the rate of virion attachment and the rate of internalization. We mathematically obtained an adequate approximation of the dynamic behavior of the virions on the surface of the cells and presented their transit rate profiles. A simplifying approximation of a constant cell concentration allowed us to obtain a closed-form solution for the profile of attached virions, which may be used to render a considerable simplification in the calculations. The proposed mechanistic approach may inspire modeling of other virus–cell systems independent of infection efficiency. It may contribute to modeling the development of novel recombinant proteins, drugs, and gene therapy vectors in mammalian cells.

Declaration of Competing Interest

The authors declare no competing interests, financial or other.

Acknowledgements

This research was financially supported by the National Natural Science Foundation of China (20876120 and 20910102037) and the Nature Science Foundation of Hubei, China (2013CFA101). We thank Professor Qi Yipeng of Wuhan University, China, for kindly providing wt *AcMNPV*.

Author contributions

Y. H. Z. conceived the project and led the research. G. E. and J. C. M. analyzed the data, developed the models and performed the calculations. W. W. and F. Z. performed all experiments. J. C. guided the performing of the FCM detections. Y. H. Z., G. E. and J. C. M. discussed the results and contributed to the final manuscript.

Ethical statement

This article does not contain any studies with human participants or animals performed by any of the authors.

Open access

Appendix A

Constant cell-based calculations

$$C_{ip}(t) = C_0 \cdot (1 - exp\{k_i(\beta - V_0)[t - ln|[\beta exp(\delta t) - V_0]/(\beta - V_0)|/\delta]\}) \quad (A1)$$

$$C_v(t) = C_0 \cdot exp\{k_i(\beta - V_0)[t - ln|[\beta exp(\delta t) - V_0]/(\beta - V_0)|/\delta]\} \quad (A2)$$

Under our assumptions we have:

$$C_{id}(t) = \begin{cases} 0 & 0 \le t \le t_e \\ k_w x(t - t_e) & t_e < t \end{cases} \quad (19)$$

Hence, applying [A1], [A2] we obtain closed-form solution for $C_{id}(t)$ and C_{iw}, respectively:

$$C_{id}(t) = \begin{cases} 0 & 0 \le t \le t_e \\ k_w \beta V_0[exp(\delta(t - t_e)) - 1]/[\beta \cdot exp(\delta(t - t_e)) - V_0] & t_e \le t \end{cases} \quad (A3)$$

$$\begin{aligned} C_{iw}(t) &= C_{ip}(t) - C_{id}(t) \\ &= C_0 \cdot \left(1 - exp\left\{k_i(\beta - V_0)\left[t - ln\left|[\beta exp(\delta t) - V_0]\Big/(\beta - V_0)\right|/\delta\right]\right\}\right) \\ &\quad - \begin{cases} 0 & 0 \le t \le t_e \\ k_w \beta V_0[exp(\delta(t - t_e)) - 1]\Big/[\beta \cdot exp(\delta(t - t_e)) - V_0] & t_e < t \end{cases} \end{aligned} \quad (A4)$$

References

Asad, A.S., Ayala, M.A.M., Gottardo, M.F., Zuccato, C., Candia, A.J.N., Zanetti, F., Seilicovich, A., Candolfi, M., 2017. Viral gene therapy for breast cancer: progress and challenges. Expert Opin. Biol. Ther. 17, 945–959. https://doi.org/10.1080/14712598.2017.1338684.

Binnicker, M.J., 2020. Emergence of a Novel Coronavirus Disease (COVID-19) and the Importance of Diagnostic Testing: Why Partnership between Clinical Laboratories, Public Health Agencies, and Industry Is Essential to Control the Outbreak. Clin. Chem. https://doi.org/10.1093/clinchem/hvaa071.

Blissard, G.W., Theilmann, D.A., 2018. Baculovirus entry and egress from insect cells. Annu. Rev. Virol. 5, 113–139. https://doi.org/10.1146/annurev-virology-092917-043356.

Boyce, F.M., Bucher, N.L.R., 1996. Baculovirus-mediated gene transfer into mammalian cells. P. Natl. Acad. Sci. USA 93, 2348–2352. https://doi.org/10.1073/pnas.93.6.2348.

Brussaard, C.P.D., 2004. Optimization of procedures for counting viruses by flow cytometry. Appl. Environ. Microb. 70, 1506–1513. https://doi.org/10.1128/AEM.70.3.1506-1513.2004.

Brussaard, C.P.D., Marie, D., Bratbak, G., 2000. Flow cytometric detection of viruses. J. Virol. Methods 85, 175–182. https://doi.org/10.1016/S0166-0934(99)00167-6.

Dee, K.U., Shuler, M.L., 1997. A mathematical model of the trafficking of acid-dependent enveloped viruses: Application to the binding, uptake, and nuclear accumulation of baculovirus. Biotechnol. Bioeng. 54, 468–490. https://doi.org/10.1002/(sici)1097-0290(19970605)54:5<468::aid-bit7>3.0.co;2-c.

Dhungel, B., Ohno, Y., Matayoshi, R., Otaki, J.M., 2013. Baculovirus-mediated gene transfer in butterfly wings in vivo: an efficient expression system with an anti-gp64 antibody. BMC Microbiol. 13, 27. https://doi.org/10.1186/1472-6750-13-27.

Dong, S., Blissard, G.W., 2012. Functional analysis of the Autographa californica multiple nucleopolyhedrovirus GP64 terminal fusion loops and interactions with membranes. J. Virol. 86, 9617–9628. https://doi.org/10.1128/JVI.00813-12.

Enden, G., Zhang, Y.H., Merchuk, J.C., 2005. A model of the dynamics of insect cell infection at low multiplicity of infection. J. Theor. Biol. 237, 257–264. https://doi.org/10.1016/j.jtbi.2005.04.013.

Espirituramirez, P., Ortegabalderas, N.Y., Sevillatapia, L., Montielmartinez, A.G., Pastorflores, A.R., Palomares, L.A., Torresvega, M.A., 2018. Gene therapy for treatment of chronic hyperammonemia in a rat model of hepatic encephalopathy. Ann. Hepatol. 17, 1026–1034. https://doi.org/10.5604/01.3001.0012.7203.

Felberbaum, R.S., 2015. The baculovirus expression vector system: A commercial manufacturing platform for viral vaccines and gene therapy vectors. Biotechnol. J. 10, 702–714. https://doi.org/10.1002/biot.201400438.

Ge, J., Jin, L., Tang, X., Gao, D., An, Q., Ping, W., 2014. Optimization of eGFP expression using a modified baculovirus expression system. J. Biotechnol. 173, 41–46. https://doi.org/10.1016/j.jbiotec.2014.01.003.

Granio, O., Porcherot, M., Corjon, S., Kitidee, K., Henning, P., Eljaafari, A., Cimarelli, A., Lindholm, L., Miossec, P., Boulanger, P., 2009. Improved adenovirus type 5 vector-mediated transduction of resistant cells by piggybacking on coxsackie B-adenovirus receptor-pseudotyped baculovirus. J. Virol. 83, 6048–6066. https://doi.org/10.1128/JVI.00012-09.

Hefferon, K.L., Oomens, A.G.P., Monsma, S.A., Finnerty, C.M., Blissard, G.W., 1999. Host cell receptor binding by baculovirus GP64 and kinetics of virion entry. Virology 258, 455–468. https://doi.org/10.1006/viro.1999.9758.

Hofmann, C., Sandig, V., Jennings, G., Rudolph, M., Schlag, P.M., Strauss, M., 1995. Efficient gene transfer into human hepatocytes by baculovirus vectors. P. Natl. Acad. Sci. USA 92, 10099–10103. https://doi.org/10.2307/2368622.

Hohmann, A.W., Faulkner, P., 1983. Monoclonal-antibodies to baculovirus structural proteins – determination of specificities by western blot analysis. Virology 125, 432–444. https://doi.org/10.1016/0042-6822(83)90214-3.

Iwami, S., Holder, B.P., Beauchemin, C.A.A., Morita, S., Tada, T., Sato, K., Igarashi, T., Miura, T., 2012. Quantification system for the viral dynamics of a highly pathogenic simian/human immunodeficiency virus based on an in vitro experiment and a mathematical model. Retrovirology 9, 18. https://doi.org/10.1186/1742-4690-9-18.

Jacobberger, J.W., Fogleman, D., Lehman, J.M., 1986. Analysis of intracellular antigens by flow cytometry. Cytometry 7, 356–364. https://doi.org/10.1002/cyto.990070410.

Jorio, H., Tran, R., Meghrous, J., Bourget, L., Kamen, A., 2006. Analysis of baculovirus aggregates using flow cytometry. J. Virol. Methods 134, 8–14. https://doi.org/10.1016/j.jviromet.2005.11.009.

Kalesnykas, G., Kokki, E., Alasaarela, L., Lesch, H.P., Tuulos, T., Kinnunen, K., Uusitalo, H., Airenne, K.J., Ylaherttuala, S., 2017. Comparative study of adeno-associated virus, adenovirus, bacu lovirus and lentivirus vectors for gene therapy of the eyes. Curr. Gene. Ther. 17, 235–247. https://doi.org/10.2174/1566523217666171003170348.

Kataoka, C., Kaname, Y., Taguwa, S., Abe, T., Fukuhara, T., Tani, H., Moriishi, K., Matsuura, Y., 2012. Baculovirus GP64-mediated entry into mammalian cells. J. Virol. 86, 2610–2620. https://doi.org/10.1128/JVI.06704-11.

Kingsley, D.H., Behbahani, A., Rashtian, A., Blissard, G.W., Zimmerberg, J., 1999. A discrete stage of baculovirus GP64-mediated membrane fusion. Mol. Biol. Cell. 10, 4191–4200. https://doi.org/10.1091/mbc.10.12.4191.

Kioukia, N., Nienow, A.W., Emery, A.N., Alrubeai, M., 1995. Physiological and environmental factors affecting the growth of insect cells and infection with baculovirus. J. Biotechnol. 38, 243–251. https://doi.org/10.1016/0168-1656(94)00128-Y.

Kost, T.A., Condreay, J.P., Jarvis, D.L., 2005. Baculovirus as versatile vectors for protein expression in insect and mammalian cells. Nat. Biotechnol. 23, 567–575. https://doi.org/10.1038/nbt1095.

Lecina, M., Soley, A., Gracia, J., Espunya, E., Lazaro, B., Cairo, J.J., Godia, F., 2006. Application of on-line OUR measurements to detect actions points to improve baculovirus-insect cell cultures in bioreactors. J. Biotechnol. 125, 385–394. https://doi.org/10.1016/j.jbiotec.2006.03.014.

Licari, P., Bailey, J.E., 1992. Modeling the population dynamics of baculovirus-infected insect cells: Optimizing infection strategies for enhanced recombinant protein yields. Biotechnol. Bioeng. 39, 432–441. https://doi.org/10.1002/bit.260390409.

Long, G., Pan, X., Kormelink, R., Vlak, J.M., 2006. Functional entry of baculovirus into insect and mammalian cells is dependent on clathrin-mediated endocytosis. J. Virol. 80, 8830–8833. https://doi.org/10.1128/JVI.00880-06.

Makkonen, K., Airenne, K.J., Ylaherttulala, S., 2015. Baculovirus-mediated gene delivery and RNAi applications. Viruses 7, 2099–2125. https://doi.org/10.3390/v7042099.

Mansouri, M., Berger, P., 2018. Baculovirus for gene delivery to mammalian cells: Past, present and future. Plasmid 98, 1–7. https://doi.org/10.1016/j.plasmid.2018.05.002.

Markovic, I., Pulyaeva, H., Sokoloff, A., Chernomordik, L.V., 1998. Membrane fusion mediated by baculovirus gp64 involves assembly of stable gp64 trimers into multiprotein aggregates. J. Cell. Biol. 143, 1155–1166. https://doi.org/10.1083/jcb.143.5.1155.

Mehalko, J.L., Esposito, D., 2016. Engineering the transposition-based baculovirus expression vector system for higher efficiency protein production from insect cells. J. Biotechnol. 238, 1–8. https://doi.org/10.1016/j.jbiotec.2016.09.002.

Monsma, S.A., Oomens, A.G.P., Blissard, G.W., 1996. The GP64 envelope fusion protein is an essential baculovirus protein required for cell-to-cell transmission of infection. J. Virol. 70, 4607–4616. https://doi.org/10.1016/0166-0934(96)02096-4.

Monteiro, F., Bernal, V., Saelens, X., Lozano, A.B., Bernal, C., Sevilla, A., Carrondo, M.J., Alves, P.M., 2014. Metabolic profiling of insect cell lines: Unveiling cell line determinants behind system's productivity. Biotechnol. Bioeng. 111, 816–828. https://doi.org/10.1002/bit.25142.

Monteiro, F., Bernal, V., Alves, P.M., 2017. The role of host cell physiology in the productivity of the baculovirus-insect cell system: Fluxome analysis of trichoplusia ni and spodoptera frugiperda cell lines. Biotechnol. Bioeng. 114, 674–684. https://doi.org/10.1002/bit.26089.

Monterio, F., Bernal, V., Chaillet, M., Berger, I., Alves, P.M., 2016. Targeted supplementation design for improved production and quality of enveloped viral particles in insect cell-baculovirus expression system. J. Biotechnol. 233, 34–41. https://doi.org/10.1016/j.jbiotec.2016.06.029.

Nwe, N., He, Q., Damrongwatanapokin, S., Du, Q., Manopo, I., Limlamthong, Y., Fenner, B.J., Spencer, L., Kwang, J., 2006. Expression of hemagglutinin protein from the avian influenza virus H5N1 in a baculovirus/insect cell system significantly enhanced by suspension culture. BMC Microbiol. 6, 16. https://doi.org/10.1186/1471-2180-6-16.

Oflynn, N.M.J., Patel, A., Kadlec, J., Jones, I.M., 2012. Improving promiscuous mammalian cell entry by the baculovirus Autographa californica multiple nuclear polyhedrosis virus. Bioscience. Rep. 33, 23–36. https://doi.org/10.1042/BSR20120093.

Ono, C., Okamoto, T., Abe, T., Matsuura, Y., 2018. Baculovirus as a tool for gene delivery and gene therapy. Viruses 10, 510. https://doi.org/10.3390/v10090510.

Padmanabhan, P., Dixit, N.M., 2011. Mathematical model of viral kinetics In vitro estimates the number of E2-CD81 complexes necessary for hepatitis C virus entry. Plos. Comput. Biol. 7 (12), e1002037. https://doi.org/10.1371/journal.pcbi.1002307.

Plonsky, I., Cho, M.S., Oomens, A.G.P., Blissard, G., Zimmerberg, J., 1999. An analysis of the role of the target membrane on the Gp64-induced fusion pore. Virology 253, 65–76. https://doi.org/10.1006/viro.1998.9493.

Saito, T., Dojima, T., Toriyama, M., Park, E.Y., 2002. The effect of cell cycle on GFPuv gene expression in the baculovirus expression system. J. Biotechnol. 93, 121–129. https://doi.org/10.1016/s0168-1656(01)00398-4.

Shang, H., Garretson, T.A., Kumar, C.S., Dieter, R.F., Cheng, X.-W., 2017. Improved pFastBac™ donor plasmid vectors for higher protein production using the Bac-to-Bac® baculovirus expression vector system. J. Biotechnol. 255, 37–46. https://doi.org/10.1016/j.jbiotec.2017.06.397.

Shen, C.F., Meghrous, J., Kamen, A., 2002. Quantitation of baculovirus particles by flow cytometry. J. Virol. Methods 105, 321–330. https://doi.org/10.1016/s0166-0934(02)00128-3.

Sinn, P.L., Hwang, Li, N., Ortiz, J.L.S., Shirazi, E., Parekh, K.R., Cooney, A.L., Schaffer, D. V., Mccray, P.B., 2017. Novel GP64 envelope variants for improved delivery to human airway epithelial cells. Gene. Ther. 24, 674–679. https://doi.org/10.1038/gt.2017.78.

Sladek, T.L., Jacobberger, J.W., 1993. Flow cytometric titration of retroviral expression vectors: comparison of methods for analysis of immunofluorescence histograms derived from cells expressing low antigen levels. Cytometry 14, 23–31. https://doi.org/10.1002/cyto.990140106.

Van Oers, M.M., Pijlman, G.P., Vlak, J.M., 2015. Thirty years of baculovirus-insect cell protein expression: from dark horse to mainstream technology. J. Gen. Virol. 96, 6–23. https://doi.org/10.1099/vir.0.067108-0.

Volkman, L.E., Goldsmith, P.A., 1985. Mechanism of neutralization of budded autographa-californica nuclear polyhedrosis-virus by a monoclonal-antibody – inhibition of entry by adsorptive endocytosis. Virology 143, 185–195. https://doi.org/10.1016/0042-6822(85)90107-2.

Wong, K.T.K., Peter, C.H., Greenfield, P.F., Reid, S., Nielsen, L.K., 1996. Low multiplicity infection of insect cells with a recombinant baculovirus: The cell yield concept. Biotechnol. Bioeng. 49, 659–666. https://doi.org/10.1002/(sici)1097-0290(19960320)49:6<659::aid-bit7>3.0.co;2-n.

Zhang, Y.H., Enden, G., Merchuk, J.C., 2005. Insect cells-baculovirus system: Factors affecting growth and low MOI infection. Biochem. Eng. J. 27, 8–16. https://doi.org/10.1016/j.bej.2005.05.013.

Zhu, N., Zhang, D., Wang, W., Li, X., Yang, B., Song, J., Zhao, X., Huang, B., Shi, W., Lu, R., Niu, P., Zhan, F., Ma, X., Wang, D., Xu, W., Wu, G., Gao, G.F., Tan, W., 2020. A novel coronavirus from patients with pneumonia in China, 2019. N. Engl. J. Med. 382, 727–733. https://doi.org/10.1056/NEJMoa2001017.